View Article Online / Journal Homepage / Table of Contents for this issue
Dynamic Article Links

Energy & Environmental Science

Cite this: *Energy Environ. Sci.*, 2012, **5**, 8937

www.rsc.org/ees

COMMUNICATION

Facile synthesis of core–shell Au@CeO_2 nanocomposites with remarkably enhanced catalytic activity for CO oxidation†

Jian Qi,[a] Jie Chen,[ab] Guodong Li,*[a] Shunxing Li,[b] Yan Gao[a] and Zhiyong Tang*[a]

Received 20th June 2012, Accepted 22nd August 2012
DOI: 10.1039/c2ee22600f

Published on 23 August 2012. Downloaded by Michigan State University on 23/01/2016 07:00:48.

Uniform Au@CeO_2 core–shell submicrospheres, in which a Au nanoparticle core is coated with a shell composed of CeO_2 nanoparticles, are easily synthesized by using hydrothermal and calcinating processes. When the Au@CeO_2 core–shell submicrospheres are used for catalytic oxidation of CO to CO_2, the full conversion temperature is decreased from over 300 °C to 155 °C with respect to the conventional supported Au–CeO_2 catalysts. Furthermore, the Au@CeO_2 core–shell submicrospheres show superior catalytic stability, and no deactivation occurs after 72 h reaction. The mechanisms of the growth and the high catalytic performance of Au@CeO_2 core–shell submicrospheres are discussed in detail.

Catalytic oxidation of CO to less toxic CO_2 is always one of the hottest topics in the field of catalysis due to its important industrial applications, such as car-exhaust emission control, chemical processing, CO_2 lasers, sensors, fuel cell technology, as well as being an ideal model reaction to study the mechanism of heterogeneous catalysis.[1] Recently, much research attention has been focused on development of novel and high-efficient catalysts for CO oxidation. Among different types of catalysts, the interest in studying the inorganic oxide supported Au catalysts has increased substantially since Haruta *et al.* discovered that small Au nanoparticles (NPs) are exceptionally active for low-temperature CO oxidation.[2] Unfortunately, the supported Au catalysts with small sizes are usually unstable and tend to sinter and grow into larger particles under the conditions of catalytic reactions,[3] leading to loss of the unique properties registered in the original NPs. Therefore, the catalytic activity of the supported Au catalysts decays rapidly, which seriously impedes their practical applications.

In order to solve the bottleneck problem of NP migration and aggregation, many strategies have been tried and generally can be classified into four categories: (1) replacement of monocomponent Au NPs with Au-based alloy NPs,[4] (2) confinement of Au NPs into mesoporous supports,[5] (3) modification of the supports,[6,7] and (4) encapsulation of Au NPs into the supports with the core–shell structure.[8] The former three methods may improve the catalytic performance to some extent, but cannot completely avoid migration and aggregation of Au NPs. As a comparison, the last one is a more effective way, because the core–shell micro-/nano-structures have high thermal stability[9] and recyclability.[10] Generally speaking, there are two typical types of shells, organic capping agents and inorganic materials. However, the organic capping molecules have low chemical and physical resistance in the catalytic reactions,[11–14] so the inorganic oxide shells with high stability have been broadly selected as the catalysts for CO oxidation. Among the various inorganic oxides including SiO_2,[15,16] TiO_2,[17–20] ZrO_2,[21,22] CeO_2,[23] SnO_2,[24–26] and Fe_2O_3,[27] CeO_2 is of special interest due to its abundant oxygen vacancy defects, high oxygen storage capacity and the relatively easy shuttles between the III and IV oxidation states, giving rise to the enhanced rates of the oxidation reaction.

It should be noted that until now only a few works have been reported on successful construction of noble metal NPs@CeO_2 core–shell composites.[23,28–30] One of the big challenges is that classical sol–gel methods[31,32] to prepare the micro-/nano-structured transition metal oxides are not suitable for CeO_2 owing to the low hydrolysis ability of Ce cations in water or alcohol solution.[33] Herein, we

[a]*Laboratory for Nanomaterials, National Center for Nanoscience and Technology, Beijing, 100190, P. R. China. E-mail: liguodong@nanoctr.cn; zytang@nanoctr.cn; Fax: +86 010-62656765*
[b]*Department of Chemistry and Environmental Science, Zhangzhou Normal University, Zhangzhou 363000, P. R. China*

† Electronic supplementary information (ESI) available. See DOI: 10.1039/c2ee22600f

Broader context

The well-defined Au@CeO_2 core–shell submicrospheres, in which a Au nanoparticle core is coated with a shell composed of CeO_2 nanoparticles, are easily synthesized by combination of hydrothermal and calcination processes. When the Au@CeO_2 core–shell submicrospheres are used for catalytic oxidation of CO to CO_2, the full conversion temperature is decreased from over 300 °C to 155 °C with respect to the conventional supported Au–CeO_2 catalysts. Furthermore, the Au@CeO_2 core–shell submicrospheres show superior catalytic stability, and no deactivation occurs after 72 h reaction. The new strategy is expected to be broadly employed to synthesize other nanomaterials with well-defined structures, which have potential applications in energy and environmental fields.

View Article Online

Published on 23 August 2012. Downloaded by Michigan State University on 23/01/2016 07:00:48.

introduce a novel and simple "self-templating" technique to fabricate the Au@CeO_2 core–shell submicrospheres. $HAuCl_4$ and $CeCl_3$ as the precursors, respectively, were mixed in the aqueous solution containing glucose and urea, subsequently the solution was placed under hydrothermal conditions to generate a dark-brown suspension, and finally the suspension was subjected to calcination to obtain the desirable products. As shown in Scheme 1, formation of the Au@CeO_2 core–shell submicrospheres involves several steps: firstly, reduction of Au^{3+} ions by glucose in the solution produces Au NPs. Then, condensation of glucose in solution under hydrothermal conditions leads to formation of amorphous carbon submicrospheres, in which the Au NP is located at the center and Ce^{3+} ions are adsorbed in the matrix shell. Finally, the spontaneously formed carbon submicrospheres are used as the sacrificial templates to generate Au@CeO_2 submicrospheres through calcination in air. Impressively, when these Au@CeO_2 submicrospheres are used as the catalysts for CO oxidation, they exhibit the considerably enhanced catalytic activity and stability with respect to the conventional supported Au–CeO_2 catalysts.[34,35]

The morphology and structure of Au@CeO_2 submicrospheres are first investigated by different characterization techniques including scanning electron microscopy (SEM), transmission electron microscopy (TEM), high-resolution transmission electron microscopy (HRTEM), high angle annular dark field scanning transmission electron microscopy (HAADF-STEM), and powder X-ray diffraction (XRD). Several important features can be recognized: (1) the prepared submicrospheres have rather uniform diameters of 178 ± 15 nm (Fig. 1a and b). (2) The magnified TEM image demonstrates that the submicrospheres have a typical core–shell structure (inset in Fig. 1b), in which a Au NP core with the diameter of about 17 nm is surrounded with a CeO_2 shell, as shown in the elemental mapping from the HAADF-STEM image (Fig. 1c). (3) The CeO_2 shell is composed of NPs with about 8–10 nm diameter (Fig. 1d), and the HRTEM image further indicates that each NP in the shell is highly crystalline with the interplanar spacings of 0.31 nm and 0.19 nm corresponding to the (111) and (220) planes of CeO_2, respectively (Fig. 1e). It is noted that the lattice spacing of Au NP cannot be observed clearly due to the thicker CeO_2 shell. (4) Finally, the crystal structure of the Au@CeO_2 submicrospheres is discerned by the powder XRD pattern (Fig. 1f). Two series of peaks, which are attributed to face-centered-cubic Au[22] (blue rhombus) and fluorite-type CeO_2 [23] (black triangles), respectively, are found for the core–shell submicrospheres.

How does the mixture of reactants evolve into the submicrospheres under the hydrothermal treatment? In order to answer this question, the intermediate products during the hydrothermal process are taken

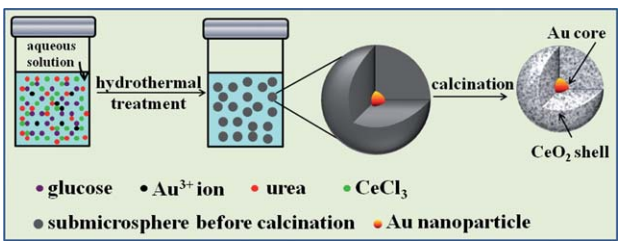

Scheme 1 Schematic illustration for controlled construction of Au@CeO_2 submicrospheres with the core–shell structure *via* the hydrothermal method.

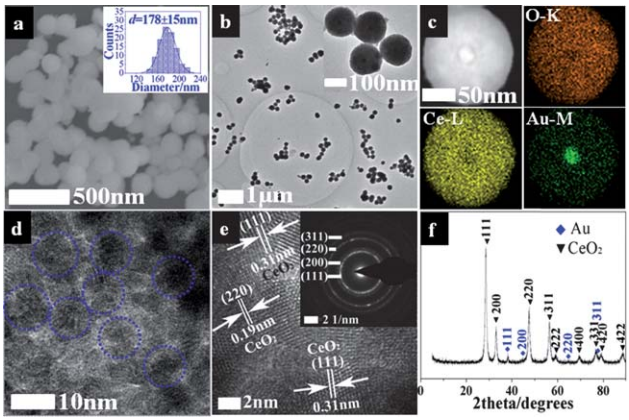

Fig. 1 (a) SEM image of Au@CeO_2 submicrospheres. The inset is the corresponding size histogram. (b) TEM image of Au@CeO_2 submicrospheres. The inset is the magnified TEM image. (c) HAADF-STEM mapping image of one submicrosphere. (d) TEM image of the CeO_2 shell of the submicrospheres. (e) HRTEM image of the submicrospheres. The inset is the selected area electron diffraction (SAED) image, indicating the polycrystalline nature of the CeO_2 shell. (f) XRD pattern of the submicrospheres.

out for characterization. Since such intermediate products are not subjected to calcination treatment, we denote them as pre-Au@CeO_2 submicrospheres. After the hydrothermal reaction only for 10 min, the pre-Au@CeO_2 core–shell submicrosphere is already formed (Fig. 2aI). With the reaction proceeding, the overall diameters of the pre-Au@CeO_2 submicrospheres gradually increase from ~60 nm to ~230 nm, while the sizes of Au NP cores remain ~17 nm (Fig. 2aI–2aIV). We also notice that the low-contrast thin shells appear and grow with a size increase of the pre-Au@CeO_2 submicrospheres

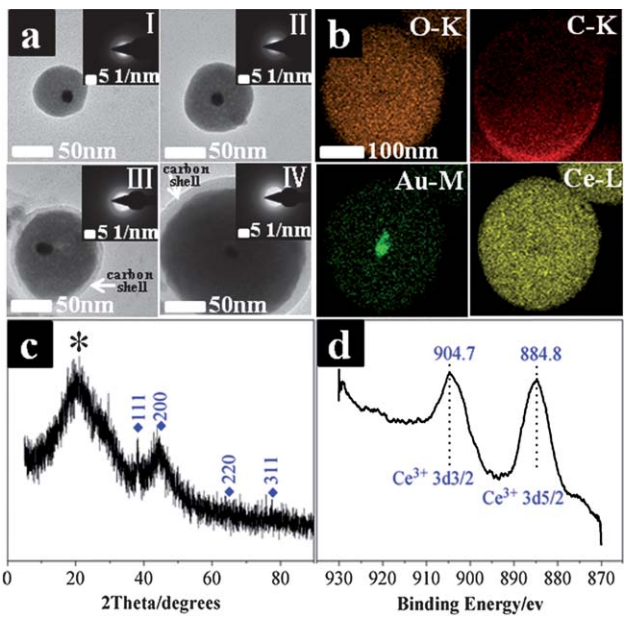

Fig. 2 (a) TEM images and corresponding SAED patterns (inset) of pre-Au@CeO_2 submicrospheres at 160 °C for different reaction times: (I) 10 min, (II) 1 h, (III) 6 h, and (IV) 20 h. (b) HAADF-STEM mapping image of the submicrosphere obtained after 20 h reaction. (c) and (d) represent the corresponding XRD and XPS patterns of (b).

 This journal is © The Royal Society of Chemistry 2012

View Article Online

Published on 23 August 2012. Downloaded by Michigan State University on 23/01/2016 07:00:48.

(arrowed parts in Fig. 2aIII). Elemental mapping by HAADF-STEM reveals that Ce and O are homogeneously distributed inside the pre-Au@CeO_2 submicrospheres, whereas the thin shell is enriched with the element C (Fig. 2b and S1†). This result indicates that adsorption of Ce ions is simultaneous with the growth of the carbon matrix, but the adsorption speed of Ce ions is relatively slower, so a pure carbon thin shell is produced. Moreover, the diffusive rings in SAED images demonstrate that the carbon matrices of all the intermediate products are amorphous (insets in Fig. 2a). The amorphous nature of carbon matrices is proved by XRD measurement of pre-Au@CeO_2 core–shell submicrospheres, in which a broad peak corresponding to amorphous carbon is distinguished (starred peak in Fig. 2c). The XRD result also tells us that the Au NP cores in the pre-Au@CeO_2 submicrospheres are already crystalline (blue rhombus peaks in Fig. 2c), but Ce is of amorphous nature and no characteristic peaks are discerned. X-ray photoelectron spectrum (XPS) analysis further shows two peaks located around 884.8 eV and 904.7 eV for pre-Au@CeO_2 submicrospheres, which coincide with the Ce^{3+} valence state[36] (Fig. 2d). This result is also consistent with the above analysis that Ce^{3+} ions are adsorbed into the carbon matrix of pre-Au@CeO_2 submicrospheres during the hydrothermal process.

Next, we investigate the role of the precursors including glucose, $CeCl_3$ and urea on formation of pre-Au@CeO_2 core–shell submicrospheres. Firstly, in the absence of glucose, the products of the dendritic morphology are obtained in the mixed solution of $CeCl_3$ and urea (Fig. S2†). Furthermore, there is no Au element to be detected. This result indicates that glucose acts as not only the source for formation of carbon submicrospheres but also the reduction agent for Au^{3+} ions. Secondly, similar submicrospheres can be produced in the mixture of glucose and $CeCl_3$, even without urea (Fig. S3†). However, the products after calcination are multi-shelled CeO_2 submicrospheres rather than Au@CeO_2 core–shell submicrospheres (Fig. S4†). One plausible explanation is that decomposition of urea under the hydrothermal condition would release OH^- ions, which provide an alkaline environment. In the solution containing urea, the functional groups of carbon submicrospheres such as carboxylic acid are deprotonated and can adsorb more Ce^{3+} ions based on the electrostatic attractions. So the content of Ce^{3+} ions in the submicrospheres decreases in the absence of urea. The calcination of carbon submicrospheres containing less of Ce^{3+} easily gives rise to generation of multi-shelled hollow structures, which is recently explored by us.[37] Also, due to the low mechanical strength of multi-shelled hollow structures, the submicrospheres are easily broken and difficult to encapsulate Au NPs (Fig. S4†). Evidently, these products are not suitable for studying the catalytic properties of nanocomposites.

Lastly, the hydrothermal products of the mixture of $HAuCl_4$ and glucose without $CeCl_3$ are examined. The core–shell submicrospheres with the sizes of around 600 nm, in which a crystalline Au NP core of about 60 nm diameter is coated with an amorphous carbon shell, are found (Fig. 3a–c). Compared with the product in the presence of Ce^{3+} ions (Fig. 2a), the relatively large size of the submicrospheres is understood, considering that adsorption with Ce^{3+} ions may slow down the growth speed of the carbon matrix. The Fourier transform infrared (FTIR) spectrum is used to identify the functional groups present in the submicrospheres (Fig. S5†). One of the most important features is appearance of the absorption bands at 1700 and 1620 cm^{-1}. These bands are attributed to C=O and C=C vibrations, which reveal that formation of carbon submicrospheres mainly

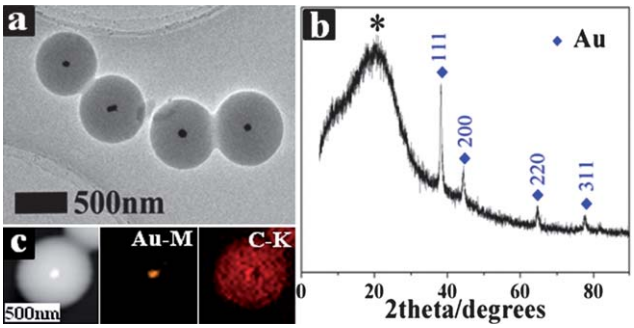

Fig. 3 (a) TEM image of core–shell submicrospheres prepared in the absence of Ce^{3+} ions. (b) and (c) represent corresponding XRD pattern and HAADF-STEM mapping images of (a). In (b), the broad peak at ~20° (star) points to the amorphous carbon,[40] while the sharp peaks (blue rhombus) stand for the crystalline Au.

originates from aromatization of glucose during the hydrothermal process.[38] It is also noted that in addition to the bands in the range of 1000–1300 cm^{-1} corresponding to the C–OH stretching and OH bending vibrations of residual glucose, there is a characteristic COO^- absorption band at 1370 cm^{-1},[39] suggesting partial oxidation of the OH or CHO functional group of glucose by Au^{3+} ions.

Altogether with the above experimental facts, we can conclude the formation mechanism of Au@CeO_2 core–shell submicrospheres (Fig. S6† and 1). The Au^{3+} ions in the solution are firstly reduced to Au^0 by glucose under the hydrothermal condition. At the same time, the dehydration–condensation reaction happens among the glucose molecules, resulting in formation and growth of the aromatic compounds and oligosaccharides around Au NPs (Fig. S6†). Urea in the solution is continuously decomposed to release OH^- ions, which promote adsorption of Ce^{3+} ions with the functional groups of submicrospheres from carbonization of glucose. Therefore, pre-Au@CeO_2 submicrospheres are synthesized. In the subsequent calcination process, carbon in the submicrospheres is burned out, and thus the size of submicrospheres shrinks from ~230 nm to ~178 nm. Simultaneously, Ce^{3+} ions in the submicrospheres are oxidized to CeO_2 (it can be confirmed by characteristic XPS peaks at 882.7 eV and 901.1 eV, corresponding to Ce^{4+} valence state,[36] Fig. S7†), leading to formation of Au@CeO_2 submicrospheres (Fig. 1). It should be pointed out that the sizes of Au NP cores are maintained around 17 nm during the calcination process, though the overall sizes of the submicrospheres are considerably decreased. This result demonstrates the excellent physical confinement of CeO_2 shells, which effectively prevent possible sintering, migration and growth of Au NP cores.

To evaluate the performance of Au@CeO_2 core–shell submicrospheres for catalytic oxidation of CO, a contrast sample is prepared by simply mixing Au NPs with the similar diameters of 14 nm and the CeO_2 submicrospheres (referred to as Au–CeO_2, see the detailed synthesis in the ESI†). Synthesis of CeO_2 submicrospheres follows the recipe of Au@CeO_2 core–shell submicrospheres except that no Au^{3+} precursors are added. In order to make such performance evaluation more comparable, all the physicochemical properties of Au–CeO_2 including the content of Au NPs, the particle size of CeO_2, specific surface area, pore volume and average pore diameter are tuned to be close to those of Au@CeO_2 (Fig. S8 and Table S1†). For example, the content of Au NPs in Au–CeO_2 and Au@CeO_2 are 1.00 wt% and 0.93 wt%, respectively (Table S1†). Both Au–CeO_2 and Au@CeO_2

View Article Online

Published on 23 August 2012. Downloaded by Michigan State University on 23/01/2016 07:00:48.

composites present the typical type IV N_2 sorption isotherms with a H3 hysteresis loop[41] (Fig. S8†), which is usually considered to be indicative of gas adsorption in the mesopores.[42,43] The corresponding specific surface areas are 80.6 and 82.5 $m^2\ g^{-1}$, pore volumes are 0.082 and 0.091 $m^3\ g^{-1}$, and average pore sizes are 2.1 and 2.2 nm with a narrow distribution for Au–CeO_2 and Au@CeO_2 composites, respectively. The presence of such mesoporous structures in both Au–CeO_2 and Au@CeO_2 submicrospheres mainly originates from the voids between CeO_2 NP aggregates (Fig. 1d), which ensure efficient mass transfer of gas molecules during the catalytic process. The evaluation of catalytic activity was performed in a fixed-bed reactor coupled online with a gas chromatograph (GC) (see the catalytic activity measurement for CO oxidation in the Experimental section of the ESI†). Fig. 4 shows the typical conversion ratio of CO as a function of reaction temperature over three catalysts under the conditions that the feed gas containing 1.0 vol% CO, 1.6 vol% O_2 and balance He was allowed to pass through the reactor at a total flow rate of 50 mL min^{-1}, corresponding to a gas hourly space velocity (GHSV) of 15 000 mL h^{-1} g_{cat}^{-1}. It can be seen that the Au@CeO_2 sample is already active at room temperature and the CO conversion ratio is about 20%, whereas at this temperature, the Au–CeO_2 shows a lower conversion of 10% and pure CeO_2 submicrosphere has no activity. With increasing the reaction temperature, the complete CO conversion temperature for the Au@CeO_2 sample is about 155 °C, which is quite remarkable.[9] As a comparison, the CO conversion ratios over Au–CeO_2 at 300 °C and pure CeO_2 at 310 °C are 87% and 76%, respectively. Evidently, the presence of Au NPs regardless of whether they are inside or outside the CeO_2 support could efficiently enhance the catalytic activity of CeO_2, demonstrating the synergetic effect of Au and CeO_2 during the catalytic process. We also would like to stress that the activity of Au–CeO_2 in this work is lower than those reported in the literature,[44–47] and this may be attributed to the below reasons: (1) Au–CeO_2 used here is not subjected to a calcination step because calcination of Au–CeO_2 would lead to a significant increase in Au particle sizes. Thus, the presence of citrate capping agent may partially suppress the activity of Au–CeO_2. (2) The sizes of Au NPs are around 14 nm and relatively large, thus leading to a low catalytic activity. Nevertheless, the temperature of full CO conversion is much lower for Au@CeO_2 core–shell submicrospheres compared with the mixed Au–CeO_2 composites. Except for possible partial removal of citrate after calcination, the remarkably higher activity of Au@CeO_2 core–shell submicrospheres is most likely attributed to the perimeter interface effects between the metal NPs and transition metal oxide supports.[48–50] Compared to the simple mixture of Au NPs and CeO_2 submicrospheres, the core–shell structure of Au@CeO_2 enables maximizing the contact area between Au NP and CeO_2, while minimizing the area of bare Au NPs. As a result, Au@CeO_2 core–shell submicrospheres show the high catalytic activity.

Also, we compared the catalytic activity of Au@CeO_2 core–shell submicrospheres with different Au contents. As shown in Fig. S9,† the order of catalytic activity is obtained as follows: 0.93% Au@CeO_2 > 0.55% Au@CeO_2 > 1.97% Au@CeO_2. The difference in the catalytic activity mainly originates from different sized Au NPs in the CeO_2 submicrospheres. The sizes of Au NPs inside both 0.55% Au@CeO_2 and 0.93% Au@CeO_2 samples are around ~17 nm (Fig. 1c and S10†), and the increase of the Au content is favorable for improvement of the catalytic activity. However, for the 1.97% Au@CeO_2 sample, the sizes of Au NPs are about 23 nm (Fig. S11†), and larger size Au NPs are not favorable for catalytic oxidation of CO, resulting in the lower catalytic activity.[51]

The stability is another important indicator to evaluate the performance of the catalysts. To make the comparison fair, we intentionally set the temperature of the catalytic reaction at the same temperature of 120 °C for both Au@CeO_2 and Au–CeO_2 samples. At 120 °C, the CO conversion ratio is around 85.1% and 20.9% on Au@CeO_2 and Au–CeO_2 catalysts, respectively. As shown in Fig. 5, no deactivation occurs for the Au@CeO_2 core–shell submicrospheres when the catalytic reaction is performed at 120 °C for 72 h. The TEM image further reveals that there are no obvious changes in the size, shape and structure of the core–shell submicrospheres (Fig. S12†). In contrast, the deactivation happens over the Au–CeO_2 catalyst, and the corresponding CO conversion ratio at 120 °C is decreased from 20.9% to 9.3% after 72 h reaction. As discussed above, many factors, *e.g.*, the size of Au NPs, the surface density of citrate capping agents and the contact area between CeO_2 and Au, would influence the activity of the catalysts. In this work, the deactivation is mainly caused by migration and sintering of Au NPs in the mixed Au–CeO_2 catalysts, which is confirmed by TEM observation that the average sizes of Au NPs are increased from original 14 nm to 18 nm after the

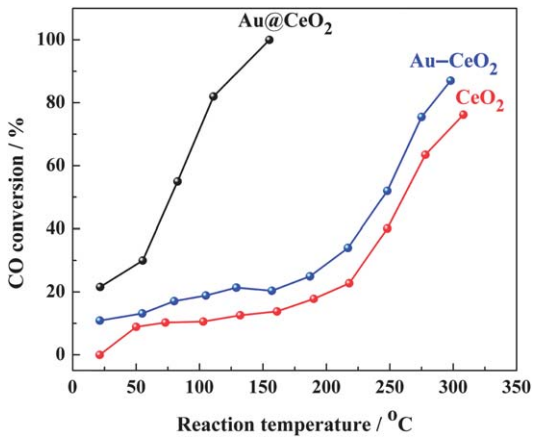

Fig. 4 Catalytic activity of Au@CeO_2, Au–CeO_2, and pure CeO_2 composites for CO oxidation. Feed gas containing 1.0 vol% CO, 1.6 vol% O_2 and balance He is at a total flow rate of 50 mL min^{-1}, corresponding to a GHSV of 15 000 mL h^{-1} g_{cat}^{-1}.

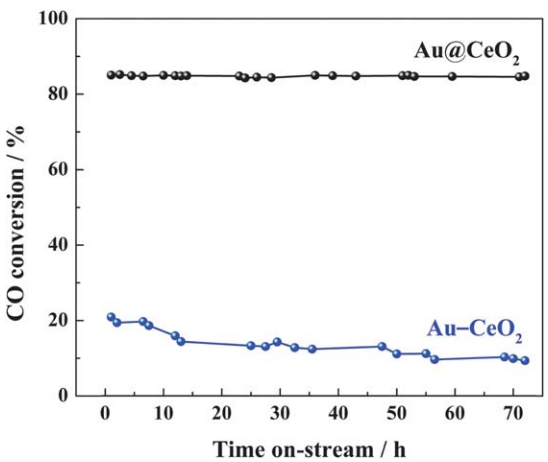

Fig. 5 Stability test of Au@CeO_2 and Au–CeO_2 at 120 °C for catalytic CO oxidation under the conditions of Fig. 4, respectively.

This journal is © The Royal Society of Chemistry 2012

View Article Online

Published on 23 August 2012. Downloaded by Michigan State University on 23/01/2016 07:00:48.

catalytic reaction (Fig. S13†). Notably, encapsulation of a single Au NP inside the CeO_2 matrix for Au@CeO_2 samples can effectively improve their stability during the catalytic process (Fig. S14†).

In conclusion, we have developed a novel and facile synthesis strategy to construct the Au@CeO_2 core–shell submicrospheres by combination of the hydrothermal and calcinating processes. The obtained Au@CeO_2 product is characterized by a Au NP core coated with a shell self-assembled by spherical CeO_2 NPs. The large contact areas between Au NP cores and CeO_2 matrices promote the catalytic oxidation of CO, while the mesopores inside CeO_2 NP aggregates are favorable for high efficiency mass transfer during the CO oxidation process, thus resulting in high catalytic activity. Furthermore, the core–shell structures can immobilize the Au NP cores and prevent possible migration and sintering, leading to superior catalytic stability. The new strategy is expected to be broadly employed to synthesize other nanomaterials of well-defined structures, which have potential applications in energy and environmental fields.

Acknowledgements

This work was supported financially by the China Postdoctoral Science Foundation (no. Y1239011QT, J.Q.), National Natural Science Foundation for Distinguished Youth Scholars of China (21025310, Z.Y.T.), National Natural Science Foundation of China (21003026, Y.G.; 20973047 and 91027011, Z.Y.T.), National Research Fund for Fundamental Key Project (2009CB930401, Z.Y.T.), and 100-Talent Program of Chinese Academy of Sciences (Z.Y.T.).

Notes and references

1 H. J. Freund, G. Meijer, M. Scheffler, R. Schlçgl and M. Wolf, *Angew. Chem., Int. Ed.*, 2011, **50**, 10064.
2 M. Haruta, N. Yamada, T. Kobayashi and S. Lijima, *J. Catal.*, 1989, **115**, 301.
3 W. C. Li, M. Comotti and F. Schüth, *J. Catal.*, 2006, **237**, 190.
4 X. Liu, A. Wang, X. Wang, T. Zhang and C. Mou, *Chem. Commun.*, 2008, 3187.
5 C. Chen, C. Y. Nan, D. S. Wang, Q. Su, H. H. Duan, X. W. Liu, L. S. Zhang, D. R. Chu, W. G. Song, Q. Peng and Y. D. Li, *Angew. Chem., Int. Ed.*, 2011, **50**, 3725.
6 Z. Ma, S. Brown, S. Overbury and S. Dai, *Appl. Catal., A*, 2007, **327**, 226.
7 K. Zhao, B. Qiao, J. Wang, Y. Zhang and T. Zhang, *Chem. Commun.*, 2011, **47**, 1779.
8 M. Cargnello, N. L. Wieder, T. Montini, R. J. Gorte and P. Fornasiero, *J. Am. Chem. Soc.*, 2010, **132**, 1402.
9 P. M. Arnal, M. Comotti and F. Schüth, *Angew. Chem., Int. Ed.*, 2006, **45**, 8224.
10 J. C. Park, J. U. Bang, J. Lee, C. H. Ko and H. Song, *J. Mater. Chem.*, 2010, **20**, 1239.
11 K. Kamata, Y. Lu and Y. N. Xia, *J. Am. Chem. Soc.*, 2003, **125**, 2384.
12 C. H. Yuan, W. A. Luo, L. N. Zhong, H. J. Deng, J. Liu, Y. T. Xu and L. Z. Dai, *Angew. Chem., Int. Ed.*, 2011, **50**, 3515.
13 M. Sindoro, Y. H. Feng, S. X. Xing, H. Li, J. Xu, H. L. Hu, C. C. Liu, Y. W. Wang, H. Zhang, Z. X. Shen and H. Y. Chen, *Angew. Chem., Int. Ed.*, 2011, **50**, 9898.
14 S. Wu, J. Dzubiella, J. Kaiser, M. Drechsler, X. H. Guo, M. Ballauff and Y. Lu, *Angew. Chem., Int. Ed.*, 2012, **51**, 2229.
15 J. Lee, J. C. Park and H. Song, *Adv. Mater.*, 2008, **20**, 1523.
16 Y. J. Wong, L. F. Zhu, W. S. Teo, Y. W. Tan, Y. H. Yang, C. Wang and H. Y. Chen, *J. Am. Chem. Soc.*, 2011, **133**, 11422.
17 I. Lee, J. B. Joo, Y. D. Yin and F. Zaera, *Angew. Chem., Int. Ed.*, 2011, **50**, 10208.
18 Z. Y. Wang and X. W. Lou, *Adv. Mater.*, 2012, **24**, 4124.
19 X. W. Lou and L. A. Archer, *Adv. Mater.*, 2008, **20**, 1853.
20 S. F. Chen, J. P. Li, K. Qian, W. P. Xu, Y. Lu, W. X. Huang and S. H. Yu, *Nano Res.*, 2010, **3**, 244.
21 R. Güttel, M. Paul, C. Galeano and F. Schüth, *J. Catal.*, 2012, **289**, 100.
22 C. Galeano, R. Güttel, M. Paul, P. Arnal, A. H. Lu and F. Schüth, *Chem.–Eur. J.*, 2011, **17**, 8434.
23 M. Cargnello, C. Gentilini, T. Montini, E. Fonda, S. Mehraeen, M. F. Chi, M. Herrera-Collado, N. D. Browning, S. Polizzi, L. Pasquato and P. Fornasiero, *Chem. Mater.*, 2010, **22**, 4335.
24 K. Yu, Z. C. Wu, Q. R. Zhao, B. X. Li and Y. Xie, *J. Phys. Chem. C*, 2008, **112**, 2244.
25 X. W. Lou, C. L. Yuan and L. A. Archer, *Adv. Mater.*, 2007, **19**, 3328.
26 X. W. Lou, C. L. Yuan and L. A. Archer, *Small*, 2007, **3**, 261.
27 H. F. Yin, Z. Ma, M. F. Chi and S. Dai, *Catal. Today*, 2011, **160**, 87.
28 M. Cargnello, N. L. Wieder, T. Montini, R. J. Gorte and P. Fornasiero, *J. Am. Chem. Soc.*, 2010, **132**, 1402.
29 T. Mitsudome, Y. Mikami, M. Matoba, T. Mizugaki, K. Jitsukawa and K. Kaneda, *Angew. Chem., Int. Ed.*, 2012, **51**, 136.
30 K. Yamazaki, T. Kayama, F. Dong and H. Shinjoh, *J. Catal.*, 2011, **282**, 289.
31 D. Djoumessi Lekeufack, A. Brioude, A. Mouti, J. G. Alauzun, P. Stadelmann, A. W. Coleman and P. Miele, *Chem. Commun.*, 2010, **46**, 4544.
32 Z. W. Seh, S. H. Liu, S. Y. Zhang, K. W. Shaha and M. Y. Han, *Chem. Commun.*, 2011, **47**, 6689.
33 Q. H. Meng, Y. H. Sun, V. Ratovelomanana-Vidal, J. P. Genêt and Z. G. Zhang, *J. Org. Chem.*, 2008, **73**, 3842.
34 V. Aguilar-Guerrero and B. Gates, *J. Catal.*, 2008, **260**, 351.
35 R. Zhang, L. Ren, A. Lu and W. Li, *Catal. Commun.*, 2011, **13**, 18.
36 Z. L. Wu, D. D. Huang and X. Z. Yang, *Vacuum*, 1998, **51**, 397.
37 Z. H. Dong, X. Y. Lai, J. E. Halpert, N. L. Yang, L. X. Yi, J. Zhai, D. Wang, Z. Y. Tang and L. Jiang, *Adv. Mater.*, 2012, **24**, 1046.
38 X. M. Sun and Y. D. Li, *Angew. Chem., Int. Ed.*, 2004, **43**, 597.
39 W. Tian, L. M. Yang, Y. Z. Xu, S. F. Weng and J. G. Wu, *Carbohydr. Res.*, 2000, **324**, 45.
40 M. Okamura, A. Takagaki, M. Toda, J. N. Kondo, K. Domen, T. Tatsumi, M. Hara and S. Hayashi, *Chem. Mater.*, 2006, **18**, 3039.
41 M. Kruk and M. Jaroniec, *Chem. Mater.*, 2001, **13**, 3169.
42 Z. A. Qiao, S. S. Brown, J. Adcock, G. M. Veith, J. C. Bauer, E. A. Payzant, R. R. Unocic and S. Dai, *Angew. Chem., Int. Ed.*, 2012, **51**, 2888.
43 K. Saravanan, K. Ananthanarayanan and P. Balaya, *Energy Environ. Sci.*, 2010, **3**, 939.
44 S. Y. Lai, Y. Qiu and S. Wang, *J. Catal.*, 2006, **237**, 303.
45 S. A. C. Carabineiro, A. M. T. Silva, G. Dražić, P. B. Tavares and J. L. Figueiredo, *Catal. Today*, 2010, **154**, 21.
46 D. Andreeva, I. Ivanov, L. Ilieva, J. W. Sobczak, G. Avdeev and T. Tabakova, *Appl. Catal., A*, 2007, **333**, 153.
47 G. Avgouropoulos, J. Papavasiliou, T. Tabakova, V. Idakiev and T. Ioannides, *Chem. Eng. J.*, 2006, **124**, 41.
48 M. Haruta, *Chem. Rec.*, 2003, **3**, 75.
49 I. X. Green, W. Tang, M. Neurock and J. T. Yates, Jr, *Science*, 2011, **333**, 736.
50 M. Haruta, *Faraday Discuss.*, 2011, **152**, 11.
51 F. Moreau and G. C. Bond, *Catal. Today*, 2006, **114**, 362.